Optical trapping via guided resonance modes in a Slot-Suzuki-phase photonic crystal lattice

Jing Ma,[1,2,*] **Luis Javier Martínez,**[1,2] **and Michelle L. Povinelli**[1]

[1]*Ming Hsieh Department of Electrical Engineering, University of Southern California, Powell Hall of Engineering, 3737 Watt Way, Los Angeles, CA 90089-0271, USA*

[2]*Both authors contributed equally to this work*

[*]*jingm@usc.edu*

http://www.usc.edu/nanophotonics

Abstract: A novel photonic crystal lattice is proposed for trapping a two-dimensional array of particles. The lattice is created by introducing a rectangular slot in each unit cell of the Suzuki-Phase lattice to enhance the light confinement of guided resonance modes. Large quality factors on the order of 10^5 are predicted in the lattice. A significant decrease of the optical power required for optical trapping can be achieved compared to our previous design.

OCIS codes: (220.0220) Optical design and fabrication; (230.5298) Photonic crystals; (350.4855) Optical tweezers or optical manipulation.

References and links

1. A. Ashkin, "Acceleration and trapping of particles by radiation pressure," Phys. Rev. Lett. **24**, 156–159 (1970).
2. K. C. Neuman and S. M. Block, "Optical trapping," Rev. Sci. Instrum. **75**, 2787–2809 (2004).
3. D. G. Grier, "A revolution in optical manipulation," Nature **424**, 810– 816 (2003).
4. J. Guck, R. Ananthakrishnan, H. Mahmood, T. J. Moon, C. C. Cunningham, and J. Käs, "The optical stretcher: A novel laser tool to micromanipulate cells," Biophys. J. **81**, 767–784 (2001).
5. D. Erickson, X. Serey, Y.-F. Chen, and S. Mandal, "Nanomanipulation using near field photonics," Lab Chip **11**, 995–1009 (2011).
6. M. L. Juan, M. Righini, and R. Quidant, "Plasmon nano-optical tweezers," Nat. Photonics **5**, 349–356 (2011).
7. A. H. J. Yang, S. D. Moore, B. S. Schmidt, M. Klug, M. Lipson, and D. Erickson, "Optical manipulation of nanoparticles and biomolecules in sub-wavelength slot waveguides," Nature **457**, 71–75 (2009).
8. M. Barth and O. Benson, "Manipulation of dielectric particles using photonic crystal cavities," Appl. Phys. Lett. **89**, 253114 (2006).
9. A. Rahmani and P. C. Chaumet, "Optical trapping near a photonic crystal," Opt. Express **14**, 6353–6358 (2006).
10. S. Lin, J. Hu, L. Kimerling, and K. Crozier, "Design of nanoslotted photonic crystal waveguide cavities for single nanoparticle trapping and detection," Opt. Lett. **34**, 3451–3453 (2009).
11. X. Serey, S. Mandal, and D. Erickson, "Comparison of silicon photonic crystal resonator designs for optical trapping of nanomaterials," Nanotechnol. **21**, 305202 (2010).
12. C. A. Mejía, A. Dutt, and M. L. Povinelli, "Light-assisted templated self assembly using photonic crystal slabs," Opt. Express **19**, 11422–11428 (2011).
13. A. R. Alija, L. J. Martínez, P. A. Postigo, J. Sánchez-Dehesa, M. Galli, A. Politi, M. Patrini, L. C. Andreani, C. Seassal, and P. Viktorovitch, "Theoretical and experimental study of the Suzuki-phase photonic crystal lattice by angle-resolved photoluminescence spectroscopy," Opt. Express **15**, 704–713 (2007).
14. C. Monat, C. Seassal, X. Letartre, P. Regreny, M. Gendry, P. R. Romeo, P. Viktorovitch, M. L. V. d'Yerville, D. Cassagne, J. P. Albert, E. Jalaguier, S. Pocas, and B. Aspar, "Two-dimensional hexagonal-shaped microcavities formed in a two-dimensional photonic crystal on an InP membrane," J. Appl. Phys. **93**, 23–31 (2003).
15. A. Taflove, *Computational electrodynamics: the finite-difference time-domain method* (Artech House, Boston, USA, 1995).

#162039 - $15.00 USD Received 24 Jan 2012; revised 24 Feb 2012; accepted 25 Feb 2012; published 8 Mar 2012

16. S. Fan, W. Suh, and J. D. Joannopoulos, "Temporal coupled-mode theory for the Fano resonance in optical resonators," J. Opt. Soc. Am. A **20**, 569–572 (2003).
17. T. Ochiai and K. Sakoda, "Dispersion relation and optical transmittance of a hexagonal photonic crystal slab," Phys. Rev. B **63**, 125107 (2001).
18. M. Galli, M. Agio, L. C. Andreani, M. Belotti, G. Guizzetti, F. Marabelli, M. Patrini, P. Bettotti, L. Dal Negro, Z. Gaburro, L. Pavesi, A. Lui, and P. Bellutti, "Spectroscopy of photonic bands in macroporous silicon photonic crystals," Phys. Rev. B **65**, 113111 (2002).
19. L. J. Martínez, A. R. Alija, P. A. Postigo, J. F. Galisteo-López, M. Galli, L. C. Andreani, C. Seassal, and P. Viktorovitch, "Effect of implementation of a Bragg reflector in the photonic band structure of the suzuki-phase photonic crystal lattice," Opt. Express **16**, 8509–8518 (2008).
20. J. D. Joannopoulos, J. N. Winn, and R. D. Meade, *Photonic Crystals: Molding the Flow of Light* (Princeton University Press, New Jersey, USA, 1995).
21. X. Letartre, J. Mouette, J. Leclercq, P. Rojo Romeo, C. Seassal, and P. Viktorovitch, "Switching devices with spatial and spectral resolution combining photonic crystal and MOEMS structures," J. Lightw. Technol. **21**, 1691 – 1699 (2003).
22. L. J. Martínez, B. Alén, I. Prieto, J. F. Galisteo-López, M. Galli, L. C. Andreani, C. Seassal, P. Viktorovitch, and P. A. Postigo, "Two-dimensional surface emitting photonic crystal laser with hybrid triangular-graphite structure," Opt. Express **17**, 15043–15051 (2009).
23. V. R. Almeida, Q. Xu, C. A. Barrios, and M. Lipson, "Guiding and confining light in void nanostructure," Opt. Lett. **29**, 1209–1211 (2004).
24. T. Yamamoto, M. Notomi, H. Taniyama, E. Kuramochi, Y. Yoshikawa, Y. Torii, and T. Kuga, "Design of a high-Q air-slot cavity based on a width-modulated line-defect in a photonic crystal slab," Opt. Express **16**, 13809–13817 (2008).
25. M. E. Beheiry, V. Liu, S. Fan, and O. Levi, "Sensitivity enhancement in photonic crystal slab biosensors," Opt. Express **18**, 22702–22714 (2010).
26. J. D. Jackson, *Classical Electrodynamics* (John Wiley & and Songs, New York, USA, 1975).
27. A. Ashkin, J. M. Dziedzic, J. E. Bjorkholm, and S. Chu, "Observation of a single-beam gradient force optical trap for dielectric particles," Opt. Lett. **11**, 288–290 (1986).
28. S. Kita, S. Hachuda, K. Nozaki, and T. Baba, "Nanoslot laser," Appl. Phys. Lett. **97**, 161108 (2010).
29. S. Kita, S. Hachuda, S. Otsuka, T. Endo, Y. Imai, Y. Nishijima, H. Misawa, and T. Baba, "Super-sensitivity in label-free protein sensing using a nanoslot nanolaser," Opt. Express **19**, 17683–17690 (2011).
30. B. B. Bakir, C. Seassal, X. Letartre, P. Viktorovitch, M. Zussy, L. D. Cioccio, and J. M. Fedeli, "Surface-emitting microlaser combining two-dimensional photonic crystal membrane and vertical Bragg mirror," Appl. Phys. Lett. **88**, 081113 (2006).
31. L. Ferrier, P. Rojo-Romeo, E. Drouard, X. Letatre, and P. Viktorovitch, "Slow bloch mode confinement in 2D photonic crystals for surface operating devices," Opt. Express **16**, 3136–3145 (2008).

1. Introduction

Optical trapping of objects with micro- and nano-scale dimensions has opened up novel opportunities in areas from physics to biology [1-4]. While optical tweezers make use of free-space beams, recent research has explored the use of integrated optical devices for particle trapping [5]. The strong evanescent fields in such micron-sized structures enable trapping on the sub-wavelength scale. Designs based on plasmonics [6], dielectric waveguides [7], and cavities [8-11] have been proposed and demonstrated for trapping of single particles. In a recent work [12], we have proposed a method to assemble 2D arrays of particles with particular, designable patterns. This process, which we call light-assisted, templated self assembly, relies on the structured light fields above a photonic-crystal slab to create an array of particle trapping locations. By changing the wavelength or polarization incident on the photonic crystal, the fields, and hence the trapping locations, can be reconfigured. This process can be used either to create tunable photonic filters or to fabricate ordered patterns of nanoparticles. In our previous work, as a proof of concept, we considered a simple, square-lattice design for the photonic crystal. The estimated power for trapping was 1mW/unit cell, limiting the feasibility of the method. However, it is known that in photonic-crystal microcavity structures, the introduction of a slot into the cavity can provide high field confinement, reducing the power required for single-particle trapping [10, 11]. In this work, we propose a novel 2D photonic crystal that exploits slot confinement to reduce the optical power for trapping of particle arrays by two orders of

#162039 - $15.00 USD Received 24 Jan 2012; revised 24 Feb 2012; accepted 25 Feb 2012; published 8 Mar 2012

magnitude.

Below, we present our novel photonic crystal structure, designed for low-power optical trapping of particle arrays. The 2D periodic structure is created by introducing a rectangular slot at the center of each unit cell of the Suzuki-phase lattice [13]. When the incident light wavelength is tuned to excite a guided resonance mode (GRM), the optical field is confined and enhanced within the slot. Meanwhile, the quality (Q) factor is increased by orders of magnitude. Our numerical simulations show that for fixed incident power, the optical force on a particle above the lattice is also enhanced by orders of magnitude, significantly reducing the power required for stable trapping. For an ideal device, stable trapping of 25-nm radius particles requires a power as low as 27 μW per unit cell, around 40 times smaller than for the simple square-lattice structures studied in our previous work [12]. We predict that a particle with dimensions smaller than the slot will be pulled inside and stably trapped. The novel lattice structure and corresponding low power requirements also open up an opportunity for experimental implementation in active structures. Using a 2D photonic crystal surface-emitting laser based on the slot Suzuki-phase design, we expect that self-adaptive trapping of 2D particle arrays may be demonstrated.

2. Structure design

The Slot-Suzuki-phase photonic crystal lattice we propose is based on the conventional Suzuki-phase (SP) lattice shown in Fig. 1(a). The Suzuki-phase lattice is obtained by starting with a triangular lattice of holes and removing selected holes to generate a rectangular lattice of $H1$ cavities [13, 14]. The Suzuki-phase lattice has different periodicities in the x and y directions, equal to $s_x = 2a$ and $s_y = \sqrt{3}a$ respectively, where a is the lattice constant of the reference triangular lattice.

Figure 1(b) illustrates the normalized transmission spectrum for vertically incident light, calculated by the three-dimensional (3D) finite-difference time-domain (FDTD) method [15]. We assume a high-refractive index Suzuki-phase lattice with relative dielectric constant ε = 11.9, hole radius r/a = 0.3 and slab thickness t/a = 0.5 resting on an oxide substrate (ε = 2.1), and immersed in a fluid with dielectric constant ε_f = 1.7. Due to the periodic modulation of the photonic crystal (PhC) slab, incident light can couple to the GRM's. Guided resonance modes are strongly confined to the slab and appear in the transmission spectrum as Fano line shapes superimposed on a Fabry-Perot background [16]. We focus in particular on Γ-point modes that are not symmetry-forbidden [17, 18]. The Γ-point is the center of the first Brillouin zone where the in-plane wave vector is zero. A band structure for a similar Suzuki-phase lattice is shown in [13, 19]. Figure 1(b) shows the four GRM's we are interested in. We label the four modes by *o1*, *o2*, *e1*, and *e2*. Figures 1(c) and (d) show the magnetic field component H_z and electric field intensity E^2 of the *o1* and *e2* resonance, respectively, in the z = 0 plane. These two, dipole-like modes are characteristic of the set. Modes were calculated by the 3D FDTD method and normalized to the maximum value in the z = 0 plane. The *o1* mode exhibits odd vector symmetry [20] with respect to the x = 0 mirror plane (*Hz* is even) and couples to a plane wave with electric field polarized along the x direction; the *e1* mode exhibits even vector symmetry with respect to the x = 0 mirror plane (*Hz* is odd) and couples to a plane wave with electric field polarized in the y direction, as has been shown experimentally [19].

We calculate Q factor for the four modes in Fig. 1(b) using 3D FDTD calculations. For a real photonic device with finite lateral size, the total Q factor depends on both vertical and lateral losses. However, for large enough structures and laser excitation spots, it is reasonable to consider only the effect of vertical loss on the Q factor [21, 22]. We model the PhC structure as infinitely periodic in the lateral direction by imposing periodic boundary conditions along the x and y directions of the unit cell in the FDTD simulation. The corresponding Q factors of the *o1* and *e2* modes are 118 and 262, respectively. In order to trap a particle in the near field

#162039 - $15.00 USD Received 24 Jan 2012; revised 24 Feb 2012; accepted 25 Feb 2012; published 8 Mar 2012

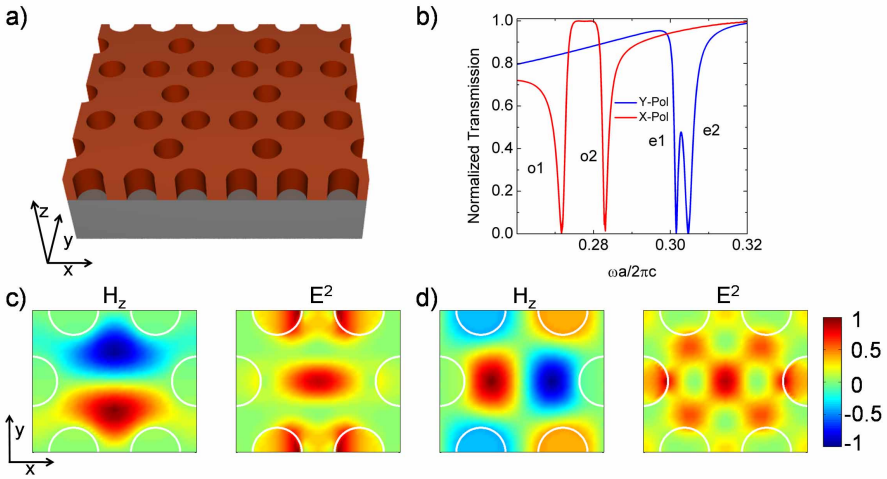

Fig. 1. a) Diagram of the Suzuki-Phase photonic crystal lattice. b) Normalized transmission spectra calculated by the finite-difference time-domain method. Red line for *x*-polarization, blue for *y*-polarization. c) *Hz*-field profile (left) and E^2 (right) of *o1* resonance. d) *Hz*-field profile (left) and E^2 (right) of *e2* resonance.

of the PhC, it is desirable to concentrate the optical power in a small surface area and to have a large Q factor [5], so as to enhance the trapping force for fixed input power. However, Figs. 1(c) and 1(d) show that the electric field intensity E^2 in the $z = 0$ plane of both the *x*-polarized and *y*-polarized dipole modes is relatively spread out across the unit cell. In order to increase the Q factor and reduce the mode area, we propose a Slot-Suzuki-phase (SSP) hybrid lattice, shown in Fig. 2(a). Rectangular slots with cross-sectional dimensions of $w_x \times w_y$ are positioned in the middle of each unit cell of the conventional SP lattice. The symbol w_x and w_y represent the slot length along the *x* and *y* axes, respectively. In the slot, the component of electric field normal to the slot boundary is enhanced due to the Maxwell continuity law [23, 24]. If the smaller dimension of the rectangular slot is along the *y* direction ($w_y < w_x$), the electric field of the *y*-polarized *e1* and *e2* modes will be enhanced. To obtain enhancement of the *x*-polarized *o1* and *o2* modes, the slot should be designed with $w_x < w_y$. In the following discussion, we focus on the case where $w_y < w_x$.

In Fig. 2(b), we plot the transmission spectrum of the SSP lattice at normal incidence for slot dimensions $w_x/a = 0.9$ and $w_y/a = 0.16$. The other structural and material parameters are identical with the above-mentioned SP lattice. We label the four Fano transmission dips as *so1*, *so2*, *se1*, and *se2*. All four modes exhibit narrower lineshapes than those in the SP lattice (Fig. 1(b)). The width of the frequency window is the same for Fig. 1(b) and Fig. 2(b). Thus, higher Q factors can be obtained which are inversely proportional to the resonance linewidths. We note that the normalized transmission of the *se1* and *se2* is expected to go to zero on resonance. The finite, non-zero values shown in the figure are a result of practical limits of the simulation time. We will focus our discussion of field localization on the *se2* mode. Figures 2(c) and (d) plot *Hz* and E^2 for the *se2* mode in the $z = 0$ plane of the SSP lattice. The electric field of the *se2* mode is well confined around the center of the slot in the *XY* plane. In fact, the modal volume for the *se2* mode in one unit cell is $V_{\text{eff}} = 2.4 \times 10^{-2}(\lambda_R/n_f)^3$, where λ_R is the resonant wavelength and n_f is the refractive index of the fluid. The mode volume per unit cell is comparable to that in PhC microcavities containing slot features [24], indicating strong confinement of the field by the slot within each unit cell of the SSP lattice. The decay length of the field intensity, for

#162039 - $15.00 USD Received 24 Jan 2012; revised 24 Feb 2012; accepted 25 Feb 2012; published 8 Mar 2012

which the value of falls to $1/e$ of the value at the slot center, are 0.28a in the x-direction, 0.09a in the y-direction, and 0.3a in the z-direction (0.05a above the PhC slab).

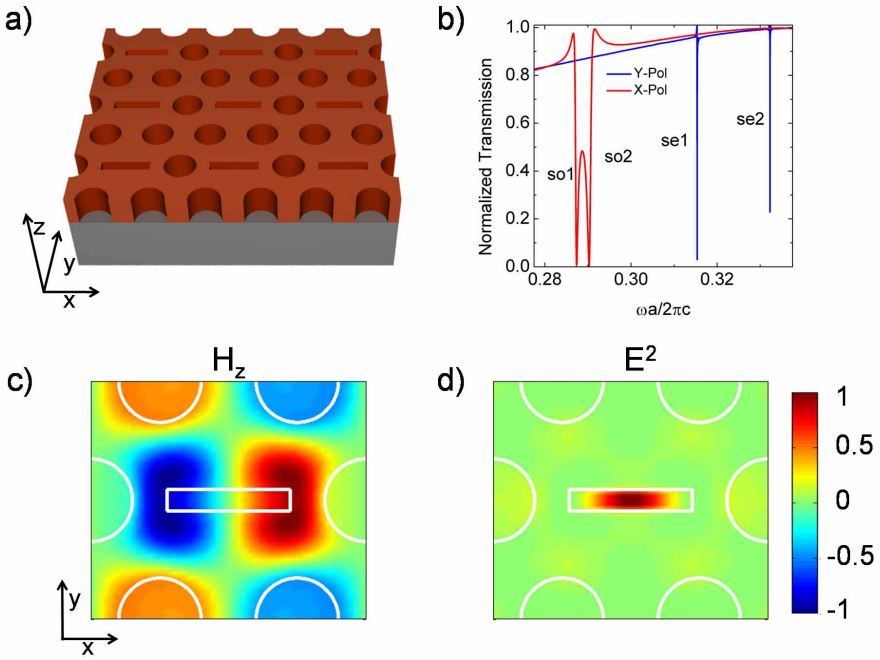

Fig. 2. a) Diagram of the Slot-Suzuki-phase hybrid lattice. b) Normalized transmission spectra. Red line for x-polarization, blue for y-polarization. c) H_z-field profile of *se2* resonance. d) E^2 field profile of *se2* resonance.

Adjusting the slot dimensions provides a flexible strategy for tuning the Q factor and resonant wavelength λ_R of the GRM's.

Varying the slot width (w_y) can dramatically increase the Q factor of the mode. In Fig. 3(a), we plot the dependence of Q on w_y for fixed w_x = 0.9a for the *se2* mode. In the limit where the slot vanishes, i.e., the conventional SP lattice with only circular holes, the Q factor for the *e2* mode is 262. By adding a narrow slot of w_y = 0.08a in the center of each unit cell, the Q factor is increased to 1750. The Q factor is further enhanced by increasing w_y and reaches a peak value of around 123,000 at w_y = 0.16a. This Q value is comparable to values obtained in square PhC lattices for coupled GRM's [25]. If the slot width w_y continues to increase beyond 0.16a, the Q factor decreases.

The slot width also affects the resonant wavelength λ_R. The blue line in Fig. 3(a) shows that λ_R linearly decreases from 1605 nm for w_y = 0.08a to 1510 nm for w_y = 0.24a with a slope of approximately -1.2. The graph is plotted assuming a fixed lattice constant a of 515 nm.

Changing the slot length (w_x) also affects the Q factor and resonant wavelength λ_R. We fix w_y = 0.16a and adjust w_x. As indicated by Fig. 3(b), the Q factor decreases from 123,000 when w_x deviates from 0.9a, but remains above 20,000 for w_x between 0.8a and 1.15a. The blue line shows that the wavelength λ_R remains relatively stable with a shift of less than 6 nm in the same w_x range. This relatively low variation can be explained by the mode distribution shown in Fig. 2(d). The electric field is tightly confined in the slot with a decay length in the x direction of 0.28a, which is less than half of the slot length ($w_x/2$ = 0.45a). Thus, the resonance profile is only lightly influenced by w_x decreasing from 1.15a to 0.8a. The choice of w_x can be considered

#162039 - $15.00 USD Received 24 Jan 2012; revised 24 Feb 2012; accepted 25 Feb 2012; published 8 Mar 2012

as an approach for fine-tuning of the dipole mode Q factor and wavelength.

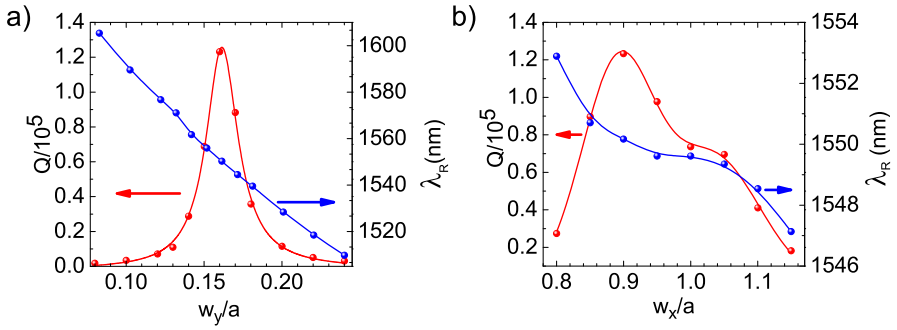

Fig. 3. a) Evolution of the Q and wavelength λ_R as a function of slot width w_y. b) Evolution of the Q and wavelength λ_R as a function of slot length w_x. Red color indicates Q; blue color indicates wavelength. Dots correspond to calculated values; lines represent a guide for the eye.

3. Optical forces

When SSP lattices with different slot dimensions are compared, the Q factor changes by orders of magnitude, while the mode profile remains similar. The component H_z has a dipole distribution and the electric field intensity is concentrated in the slot. The SSP lattice thus offers the flexibility to design a broad range of Q factors and, therefore, trapping forces. The main objective of this section is to predict the trapping capabilities of the SSP lattice with lattice constant a = 515 nm on a dielectric particle (n_{poly} = 1.60).

The trapping forces exerted on the particle are computed by integrating the Maxwell stress tensor (MST) [26] over a closed surface surrounding the particle. The forces are numerically calculated by 3D FDTD simulations. We take a rectangular solid with a surface several mesh points away from the nearest edge of the particle as the integration surface. Due to the high Q factor of the GRM, it is convenient to perform the force calculation in the time domain rather than the frequency domain. We excite the mode using a dipole source inside the slab, record the instantaneous electromagnetic fields for several optical periods, and use them to calculate the time-dependent force. We then time-average the force and normalize it to the power P coupled to the *se2* mode.

We calculate the optical force on a particle of radius varying from 25 nm to 100 nm. The particle is placed right above the center of the slot (at position x = 0, y = 0), with its bottom edge 45 nm above the top surface of the slab. Due to symmetry, the transverse force (F_{xy}) on the particle vanishes. Figure 4(a) shows the vertical force F_z/P above the SSP lattice for slot dimensions $w_x = 0.9a$ = 464 nm and w_y between $0.08a$ (41 nm) and $0.24a$ (124 nm). The force is negative, meaning that it is directed towards the slab. For all radii, the force magnitude increases to a peak value and then decreases with increasing slot width (w_y), following a similar trend as the Q factor. In the optimum case, a slot with $w_y = 0.16a$ = 82 nm enhances the force by two orders of magnitude compared to a slot with $w_y = 0.08a$ = 41 nm. The optical force increases with particle radius. For a particle of radius 25 nm, the maximum force magnitude reaches 46 pN for 1 mW power per unit cell. For a 100-nm-radius particle, the force increases to 486 pNmW^{-1}, an order of magnitude enhancement. In Fig. 4(b) we plot the dependence of force on particle radius for a particle which is at (x = 0, y = 0) and has its bottom edge 45nm above the top surface of the slab. The force magnitude increases linearly with particle radius between 25 nm and 100 nm.

#162039 - $15.00 USD Received 24 Jan 2012; revised 24 Feb 2012; accepted 25 Feb 2012; published 8 Mar 2012

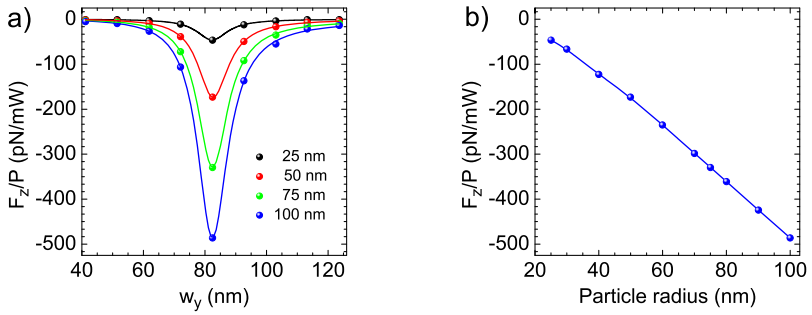

Fig. 4. a) Optical force F_z as a function of slot width w_y for four different particle radii. The slot length w_x is fixed to 464 nm. b) Optical force F_z as a function of particle radius. Dots represent the calculated values. Lines represent a guide for the eye. In both (a) and (b), the particle is at (x = 0, y = 0) and has its bottom edge 45 nm above the top surface of the slab.

To investigate the dependence of the force on particle position, we set the slot dimensions to 464 nm $\times$ 82 nm (0.9a $\times$0.16a), for which Q achieves its optimal value of 123,000. We consider a particle of radius 25 nm. The lower edge of the particle is 45 nm above the top surface of the slab (see Fig. 5(a)). We calculate the vertical force (F_z) and transverse force (F_{xy}) on the particle for each position in the XY plane. The results are shown in Figs. 5(b) and (c). The maximum magnitude of F_z is approximately 46 pNmW^{-1}, which is achieved when the particle is above the center (x = 0, y = 0). For all positions in the XY plane, the vertical force is directed towards the slab. The magnitude of the in-plane force F_{xy} is shown by the colormap in Fig. 5(c), and the force direction is indicated by blue arrows. At the center (x = 0, y = 0), the in-plane force vanishes. The strongest in-plane forces point toward the center. The maximum in-plane force for the particle is 14 pNmW^{-1} and is weaker than the maximum vertical force of 46 pNmW^{-1}. The ability to stably trap particles is thus limited by the in-plane values. Given the spatial map of the in-plane forces F_{xy} in Fig. 5(c), we can calculate a potential map in the XY plane. We calculate the potential depth ΔU by integrating the in-plane force from a reference position to each point in the XY plane. Here, the reference position is taken to be (-s_x/2, s_y/2). The choice of the reference position does not affect the relative potential depth. The potential map is shown in Fig. 5(d). The depth of the trapping potential is larger than 377 K_BT for an incident power of 1 mW per unit cell, where K_BT is the thermal energy at temperature 300 K. A figure of merit in the context of optical trapping is the stability factor $S = \Delta U/K_BT$, which reaches 377 mW^{-1} per unit cell in our device. In order to achieve a stability factor equal to 10, generally considered sufficient to achieve stable trapping despite the presence of Brownian motion [27], the power needed in the SSP lattice is 27 μW per unit cell. The power required to realize stable trapping in the SSP lattice is reduced by about 40 times compared to the power requirement in the square lattice proposed in our previous work [12]. At the equilibrium point, the trap stiffness is defined as -$\partial F_{xy}/\partial x$ along the x axis and -$\partial F_{xy}/\partial y$ along the y axis. From Fig. 5(c), we estimate trap stiffnesses of 0.12 and 0.28 pNnm^{-1}mW^{-1} for the 25 nm particle along the x and y axes, respectively, corresponding to a radial trap stiffness of 0.08 pNnm^{-1}mW^{-1} in the XY plane. Greater trap stiffness results in lower uncertainty in the trapping position. The stability factor and the radial trap stiffness we obtained exceed the values reported for dielectric trapping structures in previous works [5].

For particle diameters less than the slot width w_y, particles can be trapped inside the slot. The particle is physically confined by the slot in the y direction. We calculate the force as a function of position in the XZ plane for y = 0. Results are shown in Fig. 6(a). The force F_y, which is

#162039 - $15.00 USD Received 24 Jan 2012; revised 24 Feb 2012; accepted 25 Feb 2012; published 8 Mar 2012

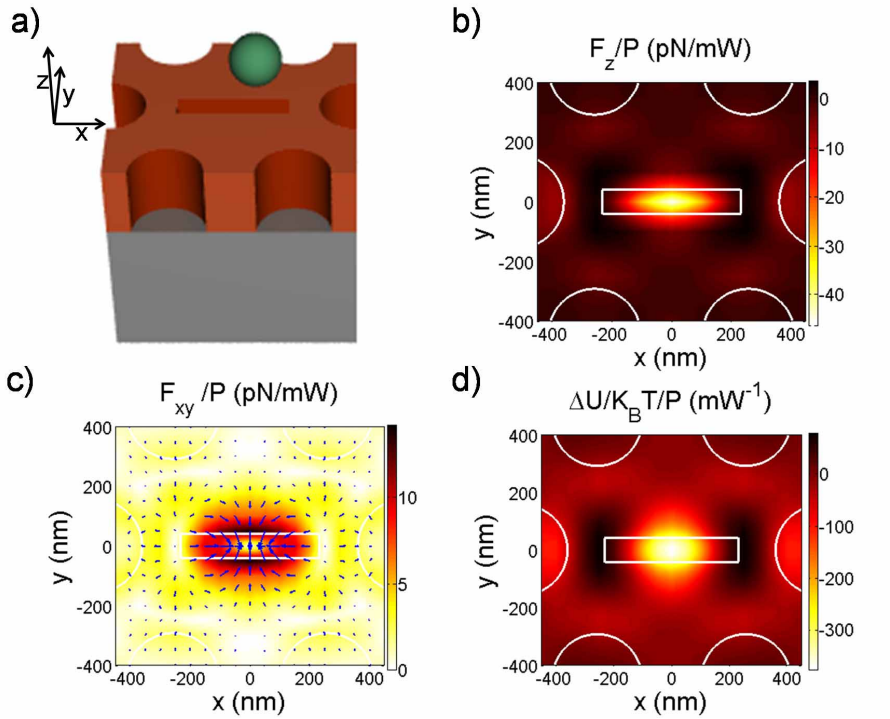

Fig. 5. a) Diagram of the Slot Suzuki-phase (SSP) lattice with a particle above. b) Vertical force F_z as a function of particle position in the*XY* plane. c) In-plane force F_{xy} as a function of position in the *XY* plane. The force magnitude is indicated by the colormap, and the force direction is shown by the blue arrows. d) Potential map in the *XY* plane. To obtain the results shown in (b), (c), and (d), we assume that the particle has a radius of 25 nm and is placed such that its bottom edge is 45 nm above the top surface of the slab.

normal to the *XZ* plane, vanishes due to symmetry, and thus, we only plot the in-plane force F_{xz}. The forces point to the center of the slot at ($x = 0$, $z = 0$) and have a maximum magnitude of 153 pNmW^{-1}. The corresponding potential map shown in Fig. 6(b) indicates that a strong trapping potential depth of more than 3500 K_BT per milliwatt per unit cell is achieved within the slot. For a particle within the slot, a power as low as 3 μW per unit cell is required for stable optical trapping. The radial trapping stiffness in the *XZ* plane is -0.34 pNnm^{-1}mW^{-1}. Within the slot, the stability and trapping stiffness are higher than outside the slot and comparable to reported values for particle trapping in other slot structures [10, 11].

The presence of a particle in the slot can affect the resonance wavelength. In a real experiment, the particles are likely to be trapped one by one, with the number increasing gradually over time. In this case, any given particle will create a negligible perturbation on the mode. As larger numbers of particles are trapped, a gradual shift of the resonance wavelength will take place, requiring a slow adjustment of the excitation laser. From perturbation theory [20], the wavelength shift scales linearly with particle density. For a density of one particle per unit cell, we estimate via FDTD simulations that the wavelength red shifts by 0.7 nm.

#162039 - $15.00 USD Received 24 Jan 2012; revised 24 Feb 2012; accepted 25 Feb 2012; published 8 Mar 2012

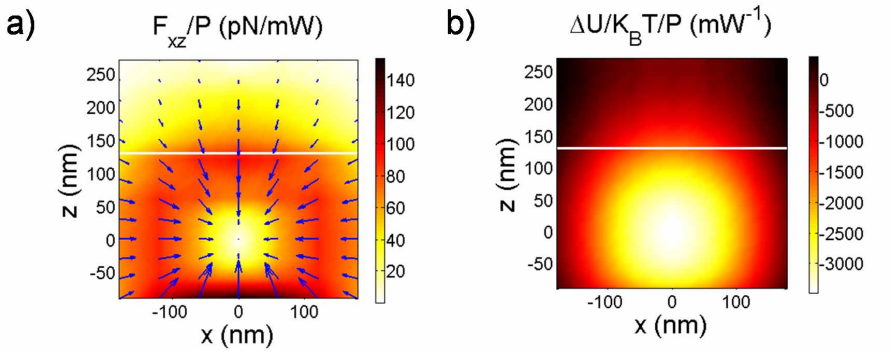

Fig. 6. a) In-plane optical force F_{xz} for a particle with radius of 25 nm. b) Optical potential map for the particle. The white line shows the top of the slot.

4. Conclusion

We have proposed a new PhC lattice for optical trapping of two-dimensional arrays of nanoparticles. Our structure is created by using the 2D Suzuki-phase PhC lattice as a base and introducing a slot into each unit cell to localize the electromagnetic field. Optimizing the slot dimensions increases the Q factor of the resonance by orders of magnitude. Optical power values as low as 27 μW per unit cell are predicted for trapping of 25 nm radius beads, a reduction of power by about 40 times relative to our previous work. Once the particle is on the slot, optical power of 3 μW per unit cell is required for the stable optical trapping. Our Slot-Suzuki-Phase lattice is a promising candidate for carrying out light-assisted templated self assembly processes.

The low power requirements for trapping suggest to use of active materials for this purpose. Slot photonic crystal microcavity lasers have been demonstrated with output optical power as high as 150 μW, and some evidence suggests possible optical trapping effects in such structures [28, 29]. The Slot-Suzuki-phase structure we propose here provides a way of effectively combining multiple slot PhC microcavities into a high-Q structure with extended area. Further improvement of the design can be achieved by band engineering techniques, as well as by combining the photonic crystal with a bottom Bragg reflector [30, 31]. In such a device, we expect that the laser may self-adapt, adjusting its own lasing wavelength in response to the resonance shift induced by trapped particles.

Acknowledgments

The authors thank Chenxi Lin and Ningfeng Huang for help with simulations and Camilo A. Mejia and Eric Jaquay for fruitful discussions. This work was funded by the Army Research Office under Award No. 56801-MS-PCS. Computing resources were provided by the USC HPCC.

#162039 - $15.00 USD Received 24 Jan 2012; revised 24 Feb 2012; accepted 25 Feb 2012; published 8 Mar 2012